Journal of Macromolecular Science, Part A
Publication details, including instructions for authors and subscription information:
http://www.informaworld.com/smpp/title~content=t713597274

Thermal Physical Characteristics of High-Performance Ablative Composites

Merrill L. Minges[a]
[a] U.S. Air Force Materials Laboratory, Wright-Patterson Air Force Base, Ohio

To cite this Article Minges, Merrill L.(1969) 'Thermal Physical Characteristics of High-Performance Ablative Composites', Journal of Macromolecular Science, Part A, 3: 4, 613 — 639
To link to this Article: DOI: 10.1080/10601326908053832
URL: http://dx.doi.org/10.1080/10601326908053832

J. MACROMOL. SCI.–CHEM., A3(4), pp. 613-639, July, 1969

Thermal Physical Characteristics of High-Performance Ablative Composites

MERRILL L. MINGES

U.S. Air Force Materials Laboratory
Wright-Patterson Air Force Base, Ohio

SUMMARY

The differential equations describing the thermochemical ablation-in-depth process and the boundary layer transport processes which couple at the ablative surface are presented. Physical interpretations of the relationships are given along with the results of sensitivity analyses which pinpoint the properties of importance in ablation performance predictions. Char thermophysical properties are shown to have a considerable influence. Based on this observation, comparisons and discussion of recent ablative char thermal conductivity results are given for high-performance carbon-phenolic and graphite-phenolic composites. Physical and chemical changes in the chars which influence the thermal transport properties are summarized and recommendations offered concerning the use of the information in ablation predictions. Finally, the important thermal and aerodynamic forces which may lead to thermomechanical and thermostructural erosion of the ablative are summarized.

INTRODUCTION

Analytical techniques for the prediction of thermochemical ablation performance of ablative plastic composites under wide ranges of re-entry and

rocket nozzle environments have reached a high state of refinement. Performance prediction analyses for monolithic graphitic and carbonaceous matrix composites incorporating sophisticated treatment of thermochemical and thermostructural effects are also available. Recent literature in the general field repeatedly cites the requirement for highly accurate thermodynamic, mechanical, and thermal transport property information in order to properly determine ablation performance. In some instances, the sophistication of the analytical prediction procedures has moved far ahead of physical and chemical property availability required for full utilization of the analyses. To cope with the nonavailability of important property information, a considerable number of investigators recently have exercised the performance prediction analyses varying property input parameters systematically to isolate those properties which exhibit high sensitivity in ablative erosion prediction.

The purpose of this paper is (a) to summarize in differential form the equations employed for thermochemical ablation-in-depth analyses, citing the important thermophysical properties which are required; (b) to compare and discuss recently obtained ablative char transport property information; (c) to summarize briefly the mechanical effects which lead to thermomechanical-thermostructural erosion of ablatives in severe environments.

THERMOCHEMICAL ABLATION EQUATIONS

Differential Formulation

A summary of the basic differential equations used in thermochemical ablation prediction is useful for several reasons: (a) It illustrates clearly the important physical and chemical processes occurring during ablation and in the transport of mass and energy across the boundary layer. (b) It indicates simply the property information requirements. (c) It illustrates the route of computer solution since these nonlinear shell-balance relationships are solved without explicit integration using finite element procedures.

Figure 1 gives a physical and mathematical schematic of the important processes involved. The most evident characteristic is the interaction of the in-depth ablation processes with effects in the boundary layer. Physical coupling between processes occurring in the boundary layer and within the ablative composite is made at the char layer surface. This is true mathematically also, the ablation in-depth analysis providing, among other things,

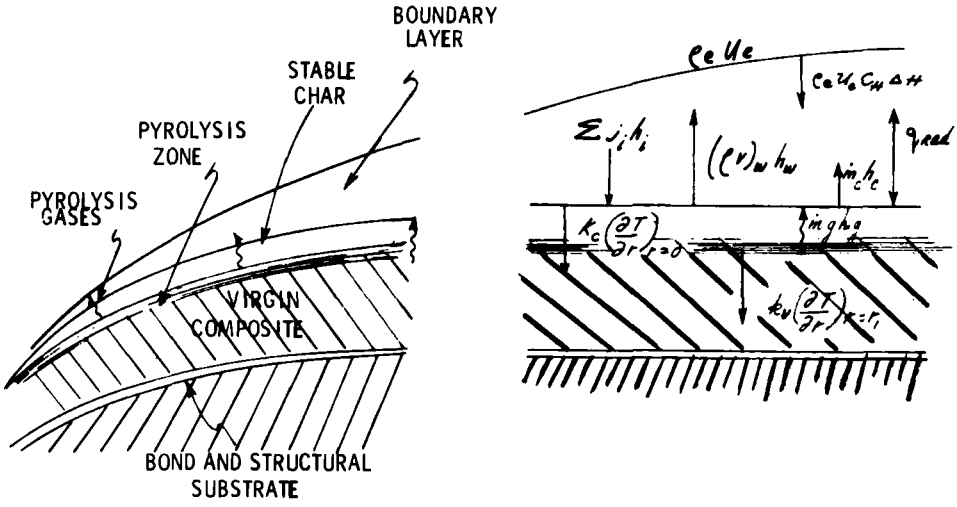

Fig. 1. In-depth charring ablation coupled with aerodynamic environment.

the necessary boundary conditions for solution of the aerodynamic boundary layer equations. The basic equations required in both regions are heat, mass, and momentum balances, both total and for individual species including allowance for homogeneous and heterogeneous chemical reaction. As indicated in Fig. 1, the following heat and mass transport processes are of first-order importance:

$k_c \left(\frac{\partial T}{\partial r}\right)_{r_0}$, $k_r \left(\frac{\partial T}{\partial r}\right)_{r_1}$	heat conduction from char, through pyrolysis zone into the virgin composite
$\dot{m}_g h_g$	heat and mass transfer associated with transpiration of the pyrolysis gases
$\dot{m}_c h_c$	heat and mass transfer due to char removal
$\left(q_{rad}\right)_{net}$	radiation heat interchange
$(\rho V)_w h_w$	"blowing" or mass and heat injection into the boundary layer

$\rho_e u_e C_H \Delta H$	heat and mass transfer across the boundary layer resulting from the enthalpy potential
$\Sigma j_i h_i$	diffusional heat and mass transfer across the boundary layer resulting from the concentration potential

In developing the equations describing the in-depth ablation process, the thermally induced pyrolysis of the ablative is usually pictured simply as in Eq. (1):

$$\text{plastic composite} \quad = \quad \text{char} + \text{gas} \tag{1}$$

A most important consequence of this assumption is that when the heat and mass balance equations are written across the pyrolysis zone, the effective properties of the zone are written as linear sums of virgin material and char properties. For example, in the case of the density-heat capacity product, the effective pyrolysis zone value is expressed simply as

$$\rho C_p = \xi_v \rho_v C_{p_v} + (1 - \xi_v)\, \rho_c C_{p_c} \tag{2}$$

where ξ_v is the volume fraction of unpyrolyzed ablative composite. Similarly, an equation of this form is written for the effective thermal conductivity. Using these effective property values, the energy balance equation for the char-pyrolysis zone is written qualitatively in the following form:

$$\left[\begin{array}{l}\text{net heat conduction}\\ \text{into the region}\end{array}\right] + \left[\begin{array}{l}\text{energy removal from}\\ \text{the region due to}\\ \text{mass transport}\end{array}\right] = \left[\begin{array}{l}\text{net storage and}\\ \text{generation of}\\ \text{energy in the region}\end{array}\right] \tag{3}$$

In the axisymmetric cylindrical coordinate system, this equation can be written in the following form using standard shell-balance techniques [1]:

$$\underbrace{\frac{\partial}{\partial r}\left(rk\frac{\partial T}{\partial r}\right)}_{\text{conduction}} + \underbrace{\frac{\partial}{\partial r}\left(\dot{m}_g H_g\right)}_{\text{mass transfer}} = r\frac{\partial}{\partial t}\left[\rho C_p T\right]$$

$$= r \left[\partial C_p \frac{\partial T}{\partial t} + C_p T \frac{\partial \rho}{\partial t} \right] \tag{4}$$

sensible enthalpy — decomposition enthalpy

The time differentiation on the right is performed to split the product into "storage" and "generation" terms.

The first term in Eq. (4) involves the effective thermal conductivity, k, of the char-pyrolysis zone which, as mentioned above, is conventionally written in the form of Eq. (2) [6]. The k value is included within the differential since it is a function of depth (r) into the ablating layer.

The second term in Eq. (4) involves the product of the total pyrolysis gas mass flow rate, $\dot{m}$, and its associated enthalpy. The mass balance or continuity equation for the decomposing plastic relates this pyrolysis gas flow rate to density change as in Eq. (5):

$$\dot{m} = 2\pi \int_{r_0}^{r_1} \left(\frac{\partial \rho}{\partial t} \right) r \, dr \tag{5}$$

Thermogravimetric analysis (TGA) data provide the necessary input to express the $\frac{\partial \rho}{\partial t}$ term in Arrhenius rate form. For phenolic resin where more than one type of reaction may be involved in the decomposition, the relationship would be of the form

$$\frac{\partial \rho}{\partial t} = \sum_i \frac{\partial \rho_i}{\partial t}, \; i = 1,2 \tag{6}$$

where

$$\frac{\partial \rho_i}{\partial t} = \rho_v \left(\frac{\rho}{\rho_v - \rho_c} \right)^{n_i} A_i e^{-E_i/RT}$$

TGA data as weight loss as a function of temperature are converted to the form of Eq. (6), by straightforward transformations of the data [3]. The more refined analyses include heating rate effects in the TGA mass loss data. The enthalpy of the gas, H_g, is the sum of the enthalpies of each gas phase species generated as a result of the pyrolysis.

The equation used is of the form

$$H_g = \sum_i c_i \int_{T_0}^{T} C_p dT \tag{7}$$

The remaining, time-differential terms of Eq. (4) account for the sensible enthalpy associated with a time-varying temperature (energy storage) and the production of heat from resin decomposition which is manifested as a density change with time (energy generation).

The charring-in-depth relationship, Eq. (4), is coupled with the boundary layer energy conservation equation and various mass conservation and kinetics equations to effect solution of the ablation performance problem; that is, prediction of surface recession, heat absorption capability, and temperature-time profiles for orbital re-entry vehicle or propulsion component environment.

The boundary layer energy equation that incorporates the terms shown in Fig. 1 can be generally written as follows:

$$\rho_e u_e C_H \left(H_R - h_w\right) + \rho_e u_e C_M \sum \left(Z_{i_e} - Z_{i_w}\right) h_i = \left(\rho V\right)_w h_w + k_c \left(\frac{\partial T}{\partial r}\right)_w + \left(q_{rad}\right)_{net} - \dot{m}_g h_g - \dot{m}_c h_c \tag{8}$$

The reduction of convective heat transfer to the ablative surface due to pyrolysis gas injection or blowing is given by the term $(\rho V)_w h_w$. This factor is most often incorporated in the first term on the left of Eq. (8) in the form of the blowing parameter, $B' = (\rho V)_w / \rho_e u_e C_M$. B' is expressible as an exponential function of the mass injection rate, $\dot{m}_g$, for laminar and turbulent multicomponent boundary layers (e.g., [4]). The driving force for the heat flux convected across the boundary layer is an enthalpy difference $(H_r - h_w)$, while the magnitude of the diffusional transport is governed by ΔZ_i, which is essentially an effective concentration differential for the multicomponent boundary layer generalized to allow for unequal mass diffusion coefficients [2, 5].

$$j_i = \rho_e u_e C_M \left(Z_{i_e} - Z_{i_w}\right)$$

The Stefan-Maxwell momentum balance relationships allow expression of the Z_i terms as functions of effective diffusion coefficients and species concentrations in the multicomponent boundary layer [2, 6]. The remaining terms in Eq. (8) require no further elaboration, except to note that surface char removal ($\dot{m}_c$) may be induced by a variety of mechanical and physical mechanisms which are discussed under thermomechanical erosion below. The relative importance of the terms in Eq. (8) varies with the vehicle environment and configuration. For example, radiative interchange is quite important for lifting-body systems, whereas for ballistic systems the various char removal mechanisms may predominate.

Ablation Prediction Sensitivities

As noted above, the primary objective in developing and solving the shell balances such as Eqs. (4) and (8) is prediction of total erosion and temperature-time histories of the regions immediately below the thermally protective layer. Once the analytical solution sequence is developed it is relatively easy to vary input properties selectively in determining the extent to which they influence erosion and temperature-time predictions. Two such studies on widely different types of ablatives illustrate the general results.

Pittman and Brewer [7] studied the recession and spatial temperature histories of a moderate-density epoxy silica composite varying the following properties systematically: char thermal conductivity, virgin material thermal conductivity, virgin material specific heat, heat of pyrolysis, temperature of pyrolysis, and pyrolysis gas specific heat. The experimental test conditions were fairly mild: subsonic, atmospheric pressure flow with an enthalpy of 3000 Btu/lb and a heating rate of 150 Btu/ft^2-sec. The results of the study showed that the virgin material and char conductivity and the pyrolysis gas specific heat affect thermal response to a greater extent than the other properties listed above. A similar study, though purely analytical in nature, was performed by Hillberg considering a high-density phenolic/carbon under turbulent flow conditions on the heat shield portion of a ballistic re-entry vehicle [8]. Of the 39 thermal and mechanical properties considered, six were found to be particularly important in the prediction of thermochemical ablation. These were: char thermal conductivity, virgin material thermal conductivity, char heat capacity, virgin material heat capacity, char density, and virgin material density. The sensitivity was consistent over a fairly wide range of re-entry vehicle ballistic coefficients. The results for the case of the char

properties are shown in Fig. 2. Increasing the char conductivity above the assumed nominal value would increase heat flux to the pyrolysis zone and also tend to decrease char surface temperature, thus decreasing reradiative heat transfer from the ablative. Both effects tend to decrease ablation efficiency. Decreasing density below the nominal value increases the char permeability and effectively decreases the amount of material available for decomposition; again ablation efficiency is reduced. Increasing the heat capacity above the nominal value has a beneficial influence on ablation performance since, on a unit weight or heat shield cross-section basis, the magnitude of the sensible enthalpy contribution increases.

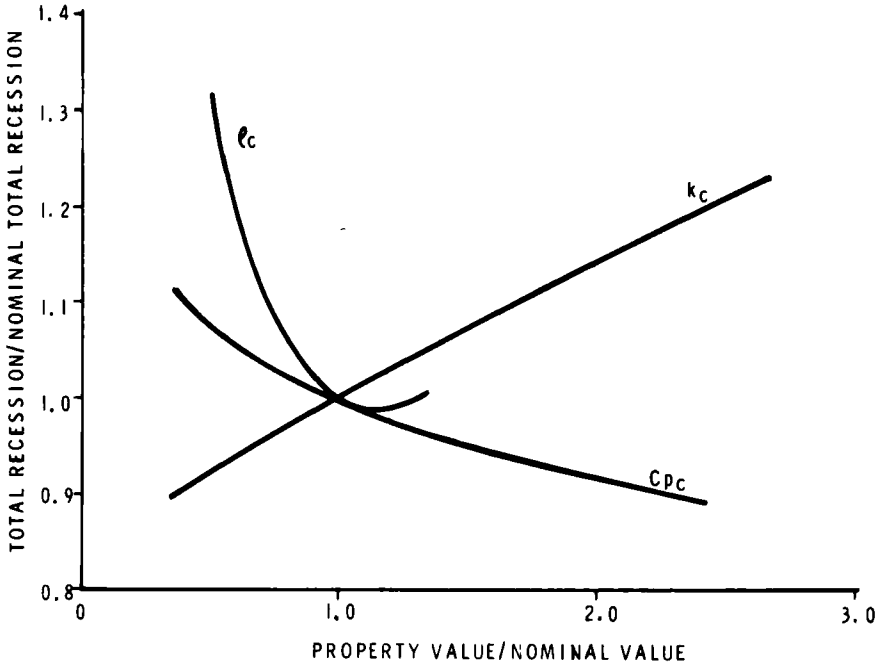

Fig. 2. Influence of thermal property variations on thermochemical ablation predictions.

In another study, Hiester and Clark [9] note that mass loss rate increases with char density, which is inconsistent with the above conclusion. It was shown by these authors that the mass loss rate increased with heating rate and stagnation pressure. Since it is expected that char density is also higher at increased heating rates, they conclude that mass loss rate

increases with char density. This does not appear to be a proper conclusion, however, since in the context of this particular study the mass loss rate and the char density were dependent variables, with stagnation pressure and heating rate or enthalpy potential being the independent correlation parameters. Rather than expressing a direct dependence of mass loss rate on char density, these authors are indicating that both char density and mass loss increase with heating rate.

Even though these studies considered widely different applications of ablatives which were themselves of distinctly different character, a common conclusion was drawn as to the considerable importance on performance of char and virgin material thermal properties. This result is not surprising in light of the important ablative processes sketched in Fig. 1 and discussed in connection with Eqs. (4) and (8).

The following section discusses ablative char thermal transport properties, considering the results of recent work in the area. This particular subject is emphasized in this paper since it is not discussed in detail by other authors in this collection of papers.

UNPYROLYZED COMPOSITE AND CHAR THERMAL PROPERTIES

Unpyrolyzed Composites

For the unpyrolyzed ablative composite, the dependence of thermal conductivity on reinforcement orientation is particularly important. Heat shield geometry, manufacturing constraints, and particularly ablation performance require large reinforcement orientation angles relative to the principal axes of the heat shield surfaces. The effect of orientation in the case of ablation performance for high-density carbon-phenolic composites has been studied extensively [10]. The orientation influence is particularly important under high-stagnation pressure-high-shear conditions in the radius and inverted chevron configurations. These configurations represent widely different reinforcement orientations with respect to the external surface of the tip and heat shield.

Thermal conductivity variations with layup are shown in Fig. 3 for the carbon-phenolic and graphite-phenolic composites described in Table 1. In addition to the considerable influence of layup angle, a high-conductivity reinforcement such as graphite tends to increase the composite conductivity. Since the resins used always have a very low conductivity relative to the reinforcement, decreasing resin percentage also increases the

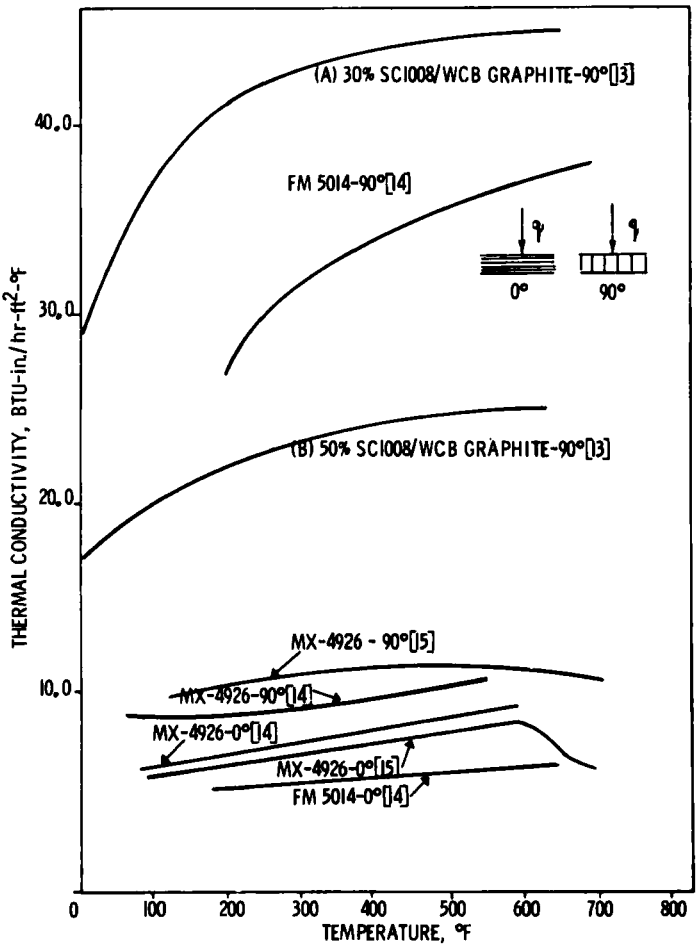

Fig. 3. Thermal conductivity of unpyrolyzed laminates.

conductivity. For a given composite there is also some disagreement in reported conductivity values from different investigators. All these typical effects are seen in Fig. 3.

Theoretically the thermal conductivity of an anisotropic composite varies with reinforcement orientation according to Eq. (9) [11]:

$$k_\theta = k_{90}° + (k_0° - k_{90}°)\cos^2\theta = k_0° \left[1 + \left(\frac{k_{90}°}{k_0°} - 1\right)\sin^2\theta\right] \tag{9}$$

Table 1. Compositional Characteristics of Typical High-Density Phenolic Resin Composites

Designation	Resin, %	Reinforcement	Composite density, lb/ft^3
MX-4926	SC-1008 (34)	CCA-1 carbon	90.6
FM-5014	CTL-91-LD (33)	WCA graphite	90.0
SoRI test	(A) SC-1008 (30)	WCB graphite	89.9
Laminate	(B) SC-1008 (50)		86.1

This form of angular dependence arises from the fact that the heat flux and grad T vectors do not maintain their orthogonal relationship in an anisotropic material. Schaefer and Dahm [12] have assigned a lesser influence of orientation angle on the thermal conductivity by assuming a $\sin \theta$ dependence rather than a $\sin^2 \theta$ dependence. The recent data of Clayton et al. [14] indicate that for the virgin composite the relationship of Eq. (9) most nearly correlates the experimental measurements particularly in the low-angle range of practical interest.

For the case of pyrolyzed ablative chars, Clayton et al. [14] found that the $\sin \theta$ relationship fit the experimental data better (within 15-30%) than the $\sin^2 \theta$ prediction. However, for partially pyrolyzed, low-temperature char (1600°R), the $\sin \theta$ prediction fit the experimental data better (within about 10%).

Ablative Chars

Char thermophysical properties are required to at least 5500°R since surface regions of the pyrolyzed ablative are heated into this range. Because the chars have varying degrees of porosity, radiation transport can contribute significantly to the overall transfer of heat through the char at high temperature. This predominance of radiative transport at high temperatures leads to rapidly increasing conductivity in this range. At lower temperatures the char conductivity is influenced by the type of reinforcement, its volume percentage, and orientation. The wide range of char conductivity values observed for nylon-phenolic, graphite-phenolic, and carbon-phenolic is indicated in Fig. 4. Generally, the higher

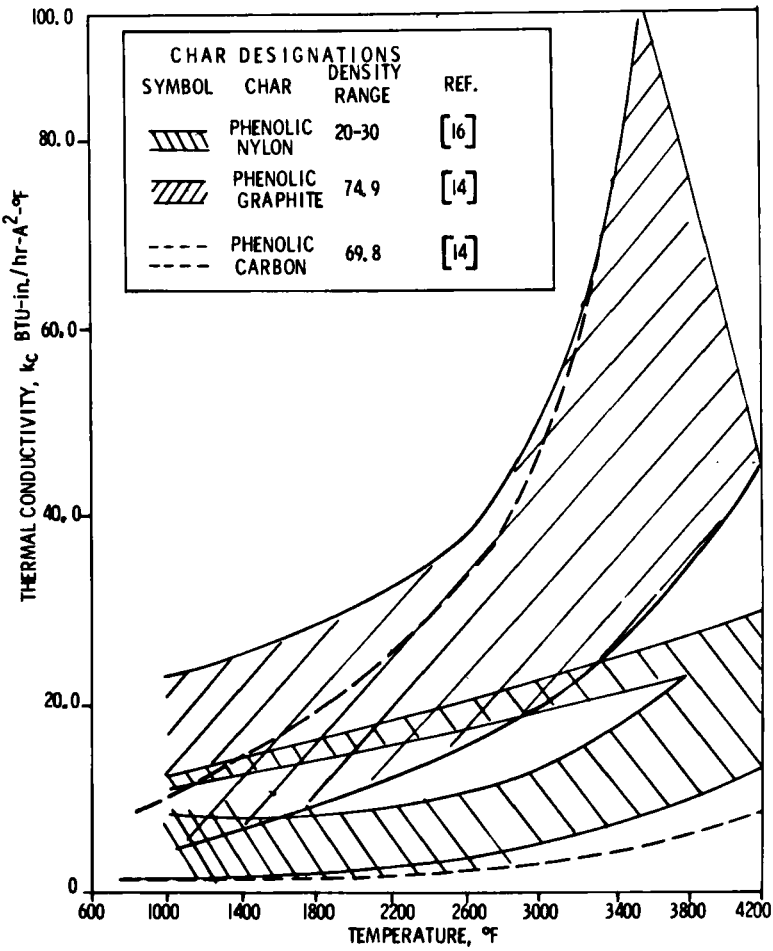

Fig. 4. Ablative char thermal conductivity.

conductivity values are for chars with 90° reinforcement orientation while the lower regions of the property band are for 0° laminations. It is noted that the strong influence of reinforcement orientation extends to high temperatures even though the solid-conduction contribution is low, indicating that void area configuaration significantly influences the magnitude of radiative transport.

In general, for any given reinforcement orientation and char structure, the conductivity temperature dependence is given by Eq. (10):

$$(k_c)_\theta = A - BT + CT^n \tag{10}$$

The linear solid conduction term coefficient, B, is negative, reflecting the fact that the solid conductivity of graphitic materials drops with temperature; the T^n term reflects the expected temperature dependency of the radiation contribution with n varying between 2.0 and 3.0. A number of authors have discussed in detail the calculation of thermal conductivity in such radiation-transmitting media. Wechsler and Glaser [17, 18], Minges [19], and Purcell and Rolinski [20] have analyzed fibrous systems composed of graphite, carbide, and refractory oxide materials and have summarized the analyses available in treating conductive and radiative heat transfer. More specifically, Pyron and Pears [21] and Nagler [16] have discussed the thermal conduction processes for phenolic-nylon chars, the conductivity of which is summarized in Fig. 4. For carbon-phenolic chars, equations for thermal conductivity as a function of temperature are discussed by Engelke et al. [22]. These authors, as well as the literature cited in their papers, give a comprehensive review of the methods for analyzing combined conductive, convective, and radiative heat transport in porous media. These papers should be consulted in estimating quantitatively the parameters of Eq. (10). The key problem though, in practical applications, is that the physical and chemical structure of the char which is the basis for evaluating the constants in Eq. (10) is either unknown or is changing rapidly with heating.

Thus, of greater relevance for re-entry and rocket nozzle applications is consideration of thermal conductivity variations with changes in thermal history. Above about 500-700°F, pyrolysis of the composite begins, the pyrolysis rate being dependent on how rapidly the temperature is increasing. After a char is formed at high temperature, changes in structure and consequently in properties may occur as a result of structural ordering. The manner in which these several effects influence the conductivity of the char is indicated schematically in Fig. 5. At lower temperatures the change in density as pyrolysis proceeds exerts a predominant influence on the conductivity, decreasing it in proportion to the density decrease. Clearly, the lower the heating rate the more complete the degradation and the greater the density decrease at any given temperature level. At high temperatures the curves may be reversed. This is because the char graphitization and structural ordering processes, which produce greatly increased conductivity, are favored by the lower heating rate. These heating curves are not retraced on cooldown since the changes in char structure produced by high-temperature

exposure are highly irreversible. The expected cooling curve conductivity is indicated by the dashed lines. The lesser slope of the cooling curve for the char experiencing a high heating rate is due to additional structural ordering occurring during the cool-down cycle, maintaining the conductivity at a higher level.

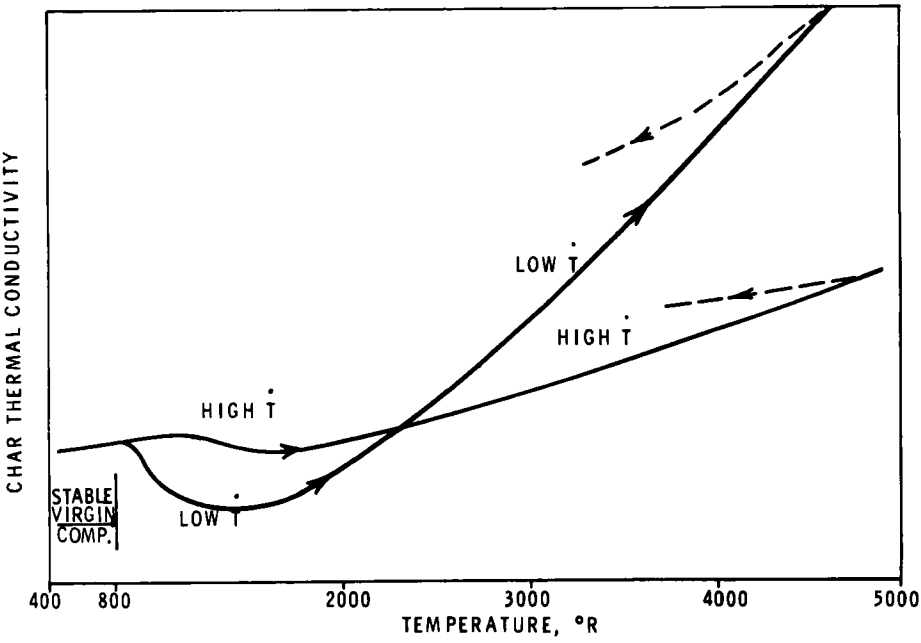

Fig. 5. Effects of heating rate on char conductivity.

Several authors have discussed different aspects of the effects outlined in Fig. 5. For example, Brazel et al. [23] discuss the generally observed characteristic that char conductivity decreases as heating rate increases and time-at-temperature decreases. They note a factor of 1.8 decrease in char conductivity measured under transient as compared with steady-state conditions. A further decrease below even the transient value of about 20% was predicted in correlating ablator performance under re-entry conditions. Nagler [16] concludes for the case of nylon-phenolic that laboratory-measured char conductivities appear conservative for atmospheric entry or one-shot propulsion devices; that is, the laboratory values are higher than those anticipated for such applications (Fig. 2 of [16]). Engelke et al.

[22] observed that furnace chars experiencing comparatively long-time soak at high temperatures had consistently higher conductivities than char produced from the same materials with short-time plasma arc exposure even though the maximum exposure temperatures were about the same. As mentioned above, during resin pyrolysis the conductivity is decreasing, with the drop in density being strongly heat rate dependent. The magnitude of the effect was estimated quantitatively by Clayton et al. [14] in discussion of results on MX-4926 carbon-phenolic char. At a maximum char temperature of 2000°R, the final char density was 71.7 for a rocket nozzle after cool-down. During steady-state ablation the density was 77.4. Under rocket nozzle start-up conditions when the heating rates are high, the char region at 2000°R had a density of 81.7. Under even more severe peak heating conditions for the same material undergoing re-entry, the density was estimated to be 87.4—very near that of the unpyrolyzed composite. Thus, depending on heating rate, the density at any given temperature level can vary by 18%, between 71.7 and 87.4.

This discussion indicates that for most re-entry and rocket nozzle ablative thermal protection applications the designs may be too conservative because the high-temperature char conductivity values are based on steady-state measurement results which are consistently high. If the in-flight ablative chars and the unpyrolyzed laminate have lower conductivity, the thermochemical erosion will be lower because the char layer will be thinner for a given temperature drop, the insulative character of the substrate also being better. The question then becomes: What are the ranges of char conductivity which can be applied for these short-time conditions which still assure design confidence? Examples of recent char data obtained under Air Force Materials Laboratory-sponsored effort are discussed below in elaborating on this point.

A recent program, carried out by the Boeing Company and Battelle Memorial Institute, examined carbon-phenolic and graphite-phenolic materials. The work was begun by studying the basic physical characteristics of ablative chars obtained from posttest hardware components. Rocket nozzle components were chosen for study based on two factors: ready availability of full-scale hardware tested under realistic conditions, and applicability of the rocket nozzle results via the more general analytical ablation-in-depth models to the re-entry case.

Nozzle segments were recovered from test firings of 120-in. solid-propellent boosters with carbon-phenolic and graphite-phenolic thermal protection components. The carbon-phenolic composite was Fiberite MX-4926 from a Thompson-Ramo-Wooldridge oblique tape-wrapped

nozzle used in the Aerojet-General Corporation 120-SS-1 motor. The graphite-phenolic composite was an H. I. Thompson rosette-molded nozzle from a solid booster.

Table 2. Char Characterization Procedures

Experimental technique	Characterization parameter
Photomicroscopy (reflection and transmission)	Gross structure phase distribution
Gas pyconometer Mercury porosimeter X-ray transmission	Density and density profiles
Helium TGA	Degree of pyrolysis
Elemental analysis	Major constituents (C and H)
X-ray diffraction	Degree of graphitization and structural ordering

A full sequence of char characterization procedures, listed in Table 2, was used. The results of this extensive characterization lead to the definition of three distinct char zones between the char surface and the virgin material region. These are summarized in Table 3.

Table 3. Carbon-Phenolic Char Zone Definition

Zone	Distinguishing features	Temperature range, °R
I	Mature char Extensive graphitization	3400-5000
II	Mature char No graphitization	2400-3400
III	Incomplete pyrolysis	1600-2400
Virgin	Room temperature Structure	500-1000

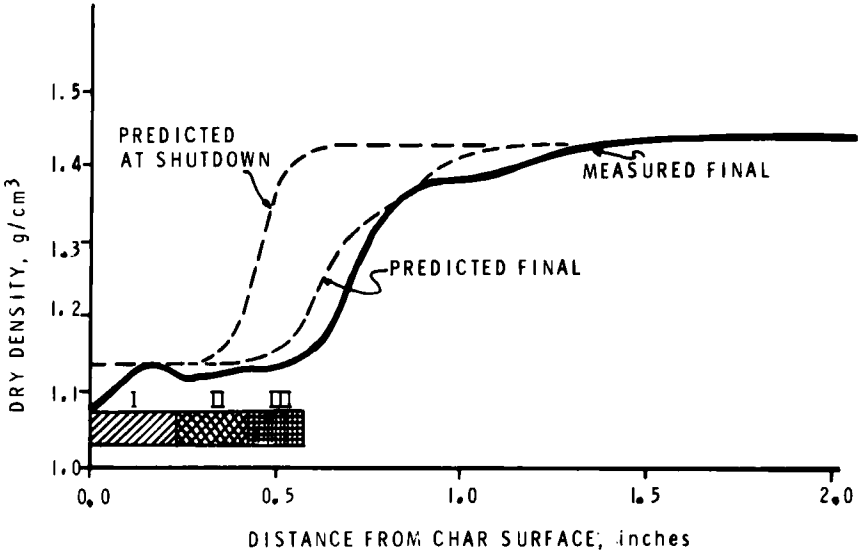

Fig. 6. Char density distribution: predicted and measured.

A graphic indication of cooling cycle history on char characteristics is given in Fig. 6. The char zones after nozzle cool-down are shown along with the predicted and measured char density distributions. The analytical predictions were performed by Aerotherm Corporation, Palo Alto, California. At nozzle shutdown there is a steep density gradient across the pyrolysis zone. However, during cool-down the pyrolysis zone existing during active ablation has been completely converted to mature char. Stated in another fashion this thermal history-heat rate effect implies that a char structure representing a certain maximum temperature during active ablation (high heating rates), say 2500°F, would correspond to a char structure experiencing only a maximum temperature of 1200°F coupled with a very low heating rate. This is because the short-time high-heating-rate exposure has the same effect on final char density as a long-time low-heating-rate exposure. This experimental observation of Fig. 6 is consistent with the heat rate effect on thermal conductivity discussed in connection with Fig. 5. That is, as the heating rate decreases the decrease in density at any given temperature is greater.

Char conductivity from this work and comparisons with results of other investigators are illustrated in Fig. 7 for the MX-4926 carbon-phenolic and in Fig. 8 for the FM-5014 graphite-phenolic. These comparisons are discussed in the following paragraphs.

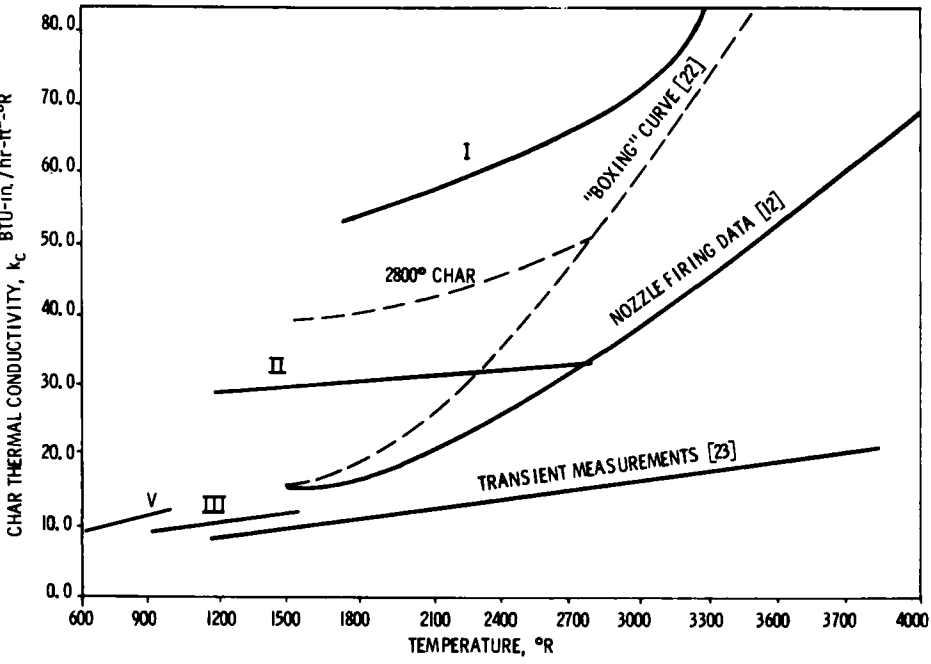

Fig. 7. Thermal conductivity of carbon-phenolic (MX-4926) ablative chars parallel to lamination.

Engelke et al. [22] have observed that the conductivity of a char material is reproducible with temperature cycling as long as the temperature at which the char was originally produced is not exceeded. Thus, a "2800° char" will follow the dotted curve shown in Fig. 7 as long as the 2800°R upper temperature point, which was the furnace preparation temperature, is not exceeded. Similar curves could be generated for chars originally produced at other temperatures. The high-temperature terminal points of these curves define the dotted "boxing" curve or locus shown in Fig. 7. The boxing curve thus represents the char conductivity which would be expected on initial heating if a virgin MX-4926 composite were charred at an infinitely slow heating rate. It is concluded by these authors that the conductivity of any char with a given heat stabilization temperature will be "boxed in" above the dotted locus curve. The relationship of the Zone I, II, and III char data with respect to the dotted locus curve is also shown in this figure. These furnace-stabilized char results confirm the general validity of the locus curve idea. The Zone III data fall below the

extrapolation between the dotted boxing curve and the unpyrolyzed composite data (V), as would be expected because unpyrolyzed resin exists in this zone. The agreement of these sets of data is striking considering that they were obtained on different lots of material, the chars were produced by different methods, and the property values were determined by different measurement techniques.

Shaefer and Dahm [12] have inferred char thermal conductivity values which exist during active ablation in a rocket nozzle test by varying the conductivity parameter in an analytical ablation-in-depth analysis until the predicted time-temperature histories matched those observed experimentally. The result for 90° orientation MX-4926 char is indicated in Fig. 7. As expected, the inferred conductivity for this case (average heating rate of about 50°R/sec) falls well below the dotted curve representing heat rate insensitivity. The transient data from General Electric [23] representing the more severe re-entry heating conditions for a similar material fall well below even the nozzle firing transient data.

Similar, recently obtained char conductivity results for the FM-5014 graphite phenolic are shown in Fig. 8 along with the inferred conductivity curve of Schaefer and Dahm for this material. These authors again varied the nozzle char conductivity until the predicted temperature-time profiles matched those observed experimentally. The data of Fig. 8 differ from those of Fig. 7 in several respects. First, because the reinforcement is graphitic, the data for the FM-5014 are all consistently higher. Second, the change in conductivity level in moving from Zone III to II to I is gradual, the three conductivity curves nearly falling on a smooth line. Although a boxing or locus curve was not available on this material, the form of the data suggests that it would lie nearly along the curve through the three char zone results. The data inferred from the high heating rate nozzle firing correlating follow the pattern suggested and discussed for Fig. 5. That is, higher conductivity than in the low heating rate case is observed at low temperatures due to different pyrolysis rates and higher conductivity at the maximum temperatures reached. The fact that the nozzle firing curve crosses the other curves at temperatures higher than that for the MX-4926 carbon-phenolic is expected since the effect of high-temperature exposure on char structure is less with the graphitized reinforcement.

In summary, the results of the above studies together with observations made recently at Washington University in connection with high-temperature char permeability determinations [24, 25] lead to the following important characteristics:

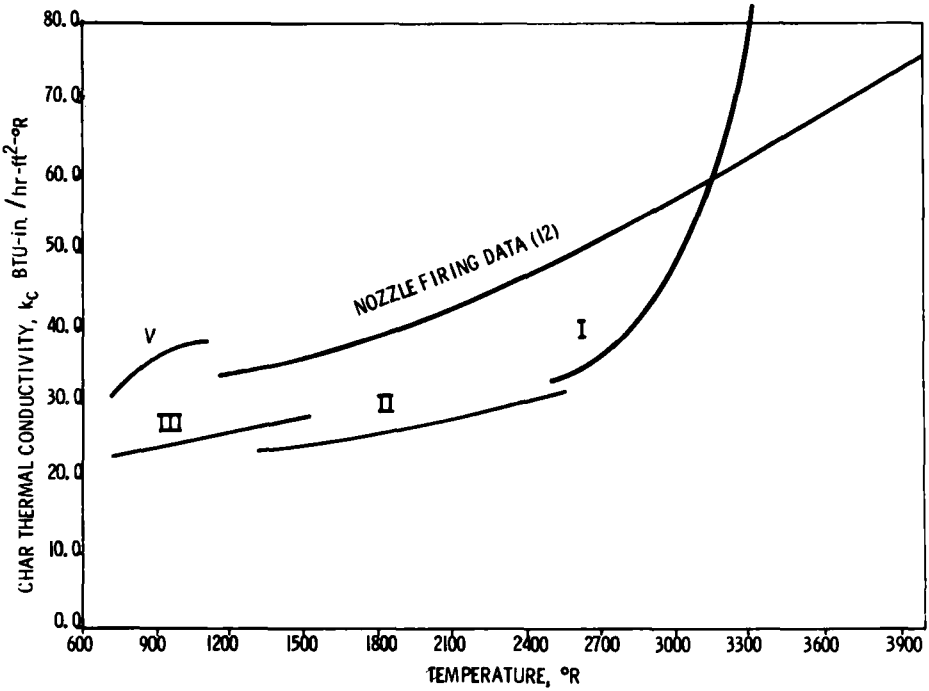

Fig. 8. Thermal conductivity of graphite-phenolic (FM-5014) ablative chars parallel to lamination.

1. In the range where there is pyrolysis of the resinous matrix material occurring (up to about 1600°F), the conductivity is influenced mainly by the density change accompanying the decomposition. The drastic chemical changes in the pyrolysis have small influence on the conductivity. As indicated in Fig. 6, it is in the pyrolysis zone where the density is changing most rapidly. For any given temperature level existing in the ablative, the composite pyrolysis is extremely heat rate-sensitive.

2. Structural ordering and graphitization of the pyrolysis residue and ungraphitized reinforcement become significant in the 2000-3000°R range. Because the rate of ordering appears to be rapid, the extent of crystallinity development is dependent primarily on maximum exposure temperature and only secondarily on time at temperature. The ordering processes appear to be essentially complete when temperatures of about 4000°R are reached.

3. Above about 3000°R there is densification of the char structure

due to the pyrolytic deposition of graphite from cracking of the pyrolysis gases as they percolate into the maximum temperature regions of the char. This deposition of a high-conductivity component increases the char conductivity significantly, particularly in the case where the original reinforcement is not graphitized (MX-4926).

4. High-temperature soak in the range of 3400-4400°R for times up to about 1 hr produces uniform graphitization of an ablative char. Pore size, which is in the range of 5-20μ, increases slightly while the size distribution about the mean decreases; however, the effect of heat soak on pore size is small.

5. Radiation transport becomes significant above 2400°R and is not strongly influenced by char thermal history since pore size and distribution stabilize rapidly. As with any composite in which radiation transport is important, the conductivity becomes a function of temperature gradient as well as temperature level. In general, the higher the gradient the higher the effective conductivity.

THERMOMECHANICAL EFFECTS

In system applications of current interest, the erosion of an ablating surface by other than thermochemical means may be important. For completeness, a brief summary of these mechanically induced processes is given below. Properties of an ablative composite and the chars produced from it other than those discussed above become important when considering processes which may lead to mechanical erosion of the surface. Thermal expansion, tensile, shear, and compressive strengths of the char are important in thermomechanical erosion. Mechanical erosion can contribute significantly to total ablative recession. Above stagnation pressures of 20 atm, surface material removed mechanically can equal that removed through thermochemical ablation. At 70 atm up to 2/3 or more of the total recession can result from mechanical effects. Thus, in such environments the thermochemical ablation predictions fall well below the observed total recession curves.

The forces acting on an ablative under severe conditions originate in at least two ways: aerodynamically induced stresses or thermally induced stresses. Specifically, the following are important: (a) momentum transport across the boundary layer producing surface shear; (b) flow field impressed pressure and surface pressure gradients in the flow direction, particularly in the stagnation region; (c) pyrolysis gas mass

transport-induced radial pressure gradients through the thickness of the ablative; and (d) normal (radial) and tangential (hoop) stresses in the ablating layer induced by high-local-temperature gradients. These effects are summarized schematically in Fig. 9, with typical magnitudes given in Table 4.

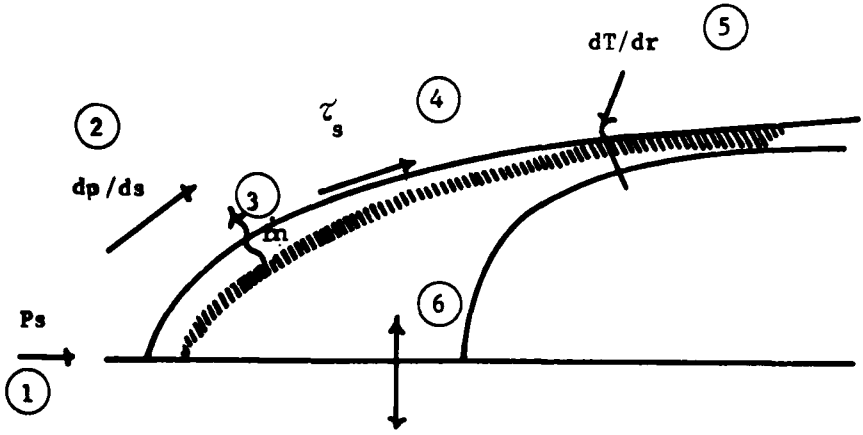

1. Aerodynamic Pressure Stress
2. Pressure Gradient Shear
3. Pyrolysis Gas Pressure
4. Aerodynamic Shear
5. Thermal Stresses
6. Acceleration Forces

Fig. 9. Thermally and aerodynamically induced forces acting on an ablative.

For example, if a quantitative determination of thermally induced stresses due to high-temperature gradients is undertaken, there is an immediate requirement for extensive mechanical and thermal property information. This approach was used recently by Schneider et al. [26]. For their particular continuum analysis of the char, thermal expansion, tensile ultimate, and compressive strengths were of prime importance in predicting the extent of thermal stress-induced mechanical erosion. The considerable uncertainties in these data limited the usefulness of the calculations to some extent. Some recent attempts to obtain "transient ablation" mechanical property data are described by Welsh and Ching[27] using carbon-phenolic and graphite phenolic materials. Their specimens were heated and

Table 4. Magnitudes of Thermomechanical Effects

Effect	Magnitude	Effect	Magnitude
Aerodynamic pressure stresses	2000 psi	Aerodynamic shear	400 lb/ft^2
Surface pressure gradient	500 atm/in.	Thermal gradients, thermal stresses	10,000°R/in., 800-12,000 psi
Pyrolysis gas pressure	50 psi	Accelerations	150 *g*

charred over 10- to 18-sec time intervals to temperatures of about 5300°R. Based on the limited data obtained, it was not possible to conclude that heating rate had a significant effect on tensile strength of the charred ablative, although the strength data were much higher than those quoted by Schneider et al. [26].

A fundamentally different approach in analysis of thermomechanical effects was used by Bishop and DiCristina [28], who considered the influences of surface shear resulting from momentum transport across the boundary layer, the shear forces generated within the char layer due to the surface pressure gradient in the flow direction, and the pyrolysis gas flow pressure. Experimental data in the form of the time dependence of spallation were obtained in high-pressure ablation tests in the wave superheater, Cornell Aeronautical Laboratory. Using computer analysis of in-depth thermochemical ablation, these authors related this time parameter to ablation depth and calculated a maximum char thickness which could be sustained for a given shear condition. Preliminary calculations indicated that this pressure gradient shear at the sonic point of a sphere cone was as high as 3500 lb/ft^2, while the aerodynamic surface shear from boundary layer momentum transport was about 275 lb/ft^2.

This analysis illustrates the apparent importance of aerodynamic pressure gradient-induced shear as compared with surface shear. It is important to note also that this is a phenomenological approach that does not require basic physical property data input in the analysis except as used in the associated thermochemical ablation computer program. However, this form of analysis is partially empirical, and systematic variations of important aerodynamic and vehicle configuration parameters will be required before generalization of the approach is established.

It is felt that phenomenological approaches such as that of Bishop and DiCristina to the mechanical erosion and spallation problem offer considerable promise in developing near-term prediction procedures for thermomechanical ablation. The nonavailability of necessary property information of the right type tends to limit the usefulness of more basic stress analyses of this problem. It is still most difficult to produce char materials with a given range of structure (e.g., density and porosity distribution) and composition (e.g., graphitization) for subsequent use in mechanical and thermal property measurements which are quantitatively traceable to active ablation conditions. Besides the limitations of furnace pyrolysis or plasma-arc generation of chars for test that were discussed earlier, it has been found that char structure is very much component geometry-sensitive. This is due primarily to the unique structural restraints imposed on the ablative in a nose tip or rocket nozzle component during flight. Plasma-arc specimens have proved of limited use in property measurement programs for this reason and also because it is difficult to retrieve high-quality specimens from the high-pressure test environments of interest. Thus, particularly in the case of mechanical properties, the type of information generated must be very closely coupled with the requirements of the particular thermomechanical analysis being used.

CONCLUSIONS

The analysis and prediction of thermochemical ablation is fairly well in hand at present, the advancements in the area being in the nature of improvements in the available analyses. Nonsimilar boundary layer solutions which allow for massive species injection, refinement of important input property information such as char thermal conductivity, and rate-sensitive pyrolysis data are examples of recent advances.

Concerning use of char conductivity information with ablation-in-depth analyses, the following guidelines are offered:

1. In the resin pyrolysis range (up to about 1600°R), the change in char conductivity is proportional to the change in total composite density as expressed via rate-dependent TGA data.

2. For re-entry and one-shot rocket nozzle applications, the heat-rate-independent or "boxing" conductivity curve represents the upper limit of the conductivity range that need be considered during the heating portion of the exposure. Heat-rate-dependent data inferred from rocket nozzle and re-entry materials performance correlations can be used as a guide in

determining how far below this locus curve one can drop for specific applications.

3. If lower-temperature char data are available, such as those from Zones III or II, they can be extrapolated with the low-temperature slope across the boxing curve for re-entry or one-shot propulsion applications where heating rates are relatively high and the char has not had previous high-temperature exposure.

4. For cool-down data the slope of the conductivity curve should be the average between the adjacent mature char curves. For example, referring to Fig. 7, if the maximum temperature experienced by a given char were 3100°R, the cooling curve slope would be the average between the Zone I and Zone II curves which bracket this 3100°R maximum temperature.

5. Important physical and chemical changes occurring in the char on initial heating are as summarized earlier.

The quantitative prediction of aerodynamically and thermomechanically induced surface erosion has not yet reached the state of refinement characterizing thermochemical analyses. A variety of forces summarized earlier become of predominant importance during different portions of an exposure cycle; thus, proper coupling between thermochemical and thermomechanical processes is complex. In the near future the empirical or phenomenological approaches to the analyses of mechanical erosion appear to offer more promise than fundamental continuum analyses because they do not rely on extensive mechanical property input information.

NOMENCLATURE

A_i pre-exponential constant
C_H heat transfer coefficient
c_i gas phase species concentrations, lb/ft^3
C_M mass transfer coefficient
C_p heat capacity, Btu/lb-°F
E_i activation energy, Btu/lb
h gas phase enthalpy, Btu/lb
H total enthalpy, Btu/lb
j diffusional mass flux, lb/hr-ft^2
k thermal conductivity, Btu-in./hr-ft^2-°F
$\dot{m}$ mass flux, lb/hr
n_i reaction order

q heat flux, Btu/hr-ft^2
r radial coordinate, in.
t time, hr
T temperature, °R
u fluid velocity, ft/sec
v velocity normal to surface, ft/sec
Z effective concentration, lb/ft^3
ξ volume fraction unpyrolyzed composite
ρ density, lb/ft^3
τ shear stress, lb/ft^2
θ angular position, spherical coordinates, deg

Subscripts

c char
e boundary layer edge
g gas phase
i species "i"
R recovery
v unpyrolyzed or virgin composite
w wall

REFERENCES

[1] R. B. Bird, W. E. Stewart, and E. N. Lightfoot, *Transport Phenomena,* Wiley, New York, 1960.
[2] R. M. Kendall, R. A. Rindal, and E. P. Bartlett, "Thermochemical Ablation," presented at AIAA Thermophysics Specialist Conf., 1965.
[3] C. B. Anderson, Aerospace Corp., *TDR-669 (S6855-20)-4*, 1966.
[4] T. R. Munson, T. R. Mascola, J. D. Brown, R. J. Spindler, and J. Klugerman, *Final Rept. NASA Contract NAS-9-4329,* Vol. 1, 1967.
[5] R. A. Rindal, D. T. Flood, and R. M. Kendall, *NASA CR-54757,* 1966.
[6] P. A. McCuen, J. W. Schaefer, R. E. Lundberg, and R. M. Kendall, U. S. Air Force, *AFRPL-TR-65-33*, 1965.
[7] C. M. Pittman and W. D. Brewer, *NASA TN D-3486*, 1966.
[8] L. H. Hillberg, *Proc. 8th Struct. Dyn. Mater. Conf.*, AIAA-ASME, 1967, pp. 278-288.

[9] N. K. Heister and C. F. Clark, *SAMPE J.*, **4**, 14-19 (1967).
[10] U. S. Air Force, Ballistic Systems Division, BSD-TR66-308, 1966.
[11] H. S. Carslaw and J. C. Jaeger, *Conduction of Heat in Solids*, Clarendon, London, 1959.
[12] J. W. Schaefer and T. J. Dahm, *NASA CR-72080*, 1966.
[13] C. D. Pears, W. T. Engelke, and J. D. Thornburgh, *AFML-TDR-64-87*, Part II, 1965.
[14] W. A. Clayton, P. B. Kennedy, R. J. Evans, J. E. Cotton, A. C. Francisco, T. J. Fabish, E. A. Eldridge, and J. F. Lagedrost, Battelle Memorial Institute, *AFML-TR-67-413*, 1968.
[15] C. D. Pears, W. T. Engelke, and J. D. Thornburgh, *AFML-TR-65-133*, 1965.
[16] R. E. Nagler, *NASA-JPL TR-32-1010*, 1967.
[17] A. E. Wechsler and P. E. Glaser, *ASD-TDR-63-574*, 1963.
[18] A. E. Wechsler and P. E. Glaser, *AFML-TR-67-251*, 1967.
[19] M. L. Minges, *ASD-TDR-63-699*, 1963.
[20] G. V. Purcell and E. J. Rolinski, *AFML-TR-67-251*, 1967.
[21] C. M. Pyron, Jr., and C. D. Pears, *ASME Paper No. 65-HT-46*, 1965.
[22] W. T. Engelke, C. M. Pyron, Jr., and C. D. Pears, *NASA CR-896*, 1967.
[23] J. P. Brazel, R. A. Tanzilli, and A. R. Begany, "Determination of the Thermal Performance of Char Under Heating Conditions Simulating Atmospheric Entry," AIAA Thermophysics Specialist Conf., 1965.
[24] E. Weger, J. Brew, and R. Schwind, *BSD-TR-66-385*, 1966.
[25] E. Weger, J. Brew, and R. Schwind, final report covering second year's work (to be published).
[26] P. J. Schneider, T. A. Dalton, and G. W. Reed, *AIAA J.*, **6**, 64-72 (1968).
[27] W. E. Welsh, Jr. and A. Ching, *AIAA J.*, **5**, 1882-1885 (1967).
[28] W. M. Bishop and V. DiCristina, *AIAA J.*, **6**, 59-63 (1968).

Accepted by editor December 24, 1968
Received for publication January 3, 1969